Available online at www.sciencedirect.com

ScienceDirect

Underground Space 6 (2021) 528–538

http://www.keaipublishing.com/undsp

A review of unloading-induced fault instability

Wei Wu

School of Civil and Environmental Engineering, Nanyang Technological University, Singapore

Received 8 August 2020; received in revised form 9 November 2020; accepted 16 November 2020
Available online 15 December 2020

Abstract

Induced seismicity associated with underground space creation and resource extraction has become a matter of global concern. However, our ability to predict and mitigate anthropogenic geohazards is still woefully inadequate. This review provides an overview of unloading-induced seismicity and highlights the mechanisms behind fault instability from a view of rock mechanics. Based on numerous fault instability cases, reduction and rotation of in situ stresses on pre-existing faults are possible causes of excavation-induced seismicity. Fault instability during resource extraction is related to many geological and operational factors, including mining depth, pore pressure, stress distribution, and production rate. Most of these cases can be explained by the Mohr–Coulomb failure criterion, and some exceptional cases could offer us new clues to improve the understanding of the mechanisms behind and the ability to predict and mitigate the induced seismic events. The current challenges include how to control remote triggering of fault instability and how to manage unseen threat of undetected faults. Emerging technologies, such as data analytics and machine learning, combining with physical models could be the next frontier for fault instability research.

Keywords: Fault instability; Underground excavation; Energy extraction; Induced seismicity

1 Introduction

In the early 20th century, underground mining was recognized as the main cause of earth tremors (Gane et al., 1946). A strong correlation between mining rate and rock burst was observed in Czechoslovakia from 1913 to 1938 (Sebik, 1963). Hundreds of mining-induced earthquakes were recorded at the gold fields in South Africa, and the 1977 local magnitude (M_L) 5.2 Klerksdorp earthquake was known as one of the largest seismic events (McGarr, Simpson, & Seeber, 2002). Early studies showed that fault instability significantly influences stress distribution and rock failure around underground excavation (Cook, 1976). In recent years, anthropogenic earthquakes have become a major obstacle to underground space creation and resource extraction. For example, a series of 112 induced earthquakes was monitored during the construction of the Gotthard Base Tunnel in Switzerland (Husen, Kissling, & von Deschwanden, 2013), and the 2015 moment magnitude (M_W) 7.8 Gorkha earthquake in Nepal was attributed to groundwater extraction (Kundu, Vissa, & Gahalaut, 2015). These geohazards have attracted wide media and public attention. However, our ability to manage the geohazard risks remains woefully inadequate. We are still witnessing numerous induced seismic events and the associated loss of lives and properties annually. Causes of geohazard occurrence can be revealed in individual cases, but each case may have specific geological and engineering conditions. Therefore, understanding the common mechanisms behind unloading-induced seismicity could provide important clues to mitigate and predict the geohazard risks.

The condition of fault failure is usually expressed based on the Mohr–Coulomb failure criterion. Fault instability occurs when the shear stress (τ) on the fault exceeds the frictional strength, which is the product of the friction coefficient (μ) and effective normal stress (σ_n'):

$$\tau = \mu\sigma_n' = \mu(\sigma_n - p), \tag{1}$$

E-mail address: wu.wei@ntu.edu.sg

https://doi.org/10.1016/j.undsp.2020.11.001

where σ_n is the normal stress, and p is the pore pressure. Here the cohesive strength of the fault is neglected under crustal conditions (Ellsworth, 2013).

Decreasing the normal stress in the unloading process is the primary cause of fault instability. The shear stress can be amplified in adjacent rocks to promote fault failure (Lu et al., 2019), but the drainage condition is less significant (Ji, Wu, & Zhao, 2019). At the onset of fault instability, the reduction rate of normal stress on the fault is higher than that of shear stress (Wu, Zhao, & Duan, 2017). After tunnel excavation, the radial stress at the tunnel perimeter approaches zero, and the vertical stress becomes the maximum principal stress (Cai, 2008). When the pore pressure is neglected, the stress changes enlarge the size of the Mohr circle and lead to a part of the circle exceeding the failure envelope (Fig. 1(a)). During gas extraction, the unequal increases in the maximum and minimum principal stresses seem to stabilize the fault inside a gas reservoir (Fig. 1(b)), and the difference between the stress changes depends on the horizontal normalized arching ratio (Soltanzadeh & Hawkes, 2008). For the fault outside the reservoir, the pressure drop enlarges the difference between the principal stresses and moves the circle closer to the failure envelope (van Wees et al., 2014), which is similar to the case shown in Fig. 1(a). For the same fault under dry and wet conditions, the friction coefficient in the wet case is smaller than that in the dry case due to water lubrication, and the presence of water promotes the instability of critically stressed faults (Dou et al., 2020).

Natural faults evolve in a dynamic and complex environment caused by unloading activities. Polymodal faulting, which is known as multiple faults moving simultaneously, under truly triaxial stresses is common in the earth (Healy et al., 2015). Unloading perturbation promotes three-dimensional interaction of these faults, which is beyond the plane strain condition of the Mohr–Coulomb failure criterion. Additionally, non-uniform fluid pressure distribution on the fault is not addressed in the failure criterion and may cause the stress state at fault failure overshooting the failure envelope (Ji et al., 2019). These exceptional cases are not predictable by the failure criterion. The mechanisms of unloading-induced fault instability are also related to shear stress transfer (Orlecka-Sikora, 2010), rupture initiation and propagation (McKinnon, 2006), overburden compaction and failure (Candela et al., 2019), as well as extreme temperature and pressure conditions if the unloading activities occur deep in the earth. Hence, a review is timely and necessary to summarize these geological and environmental factors and their influences on the mechanisms of unloading-induced seismicity and to spark our creative thinking on rediction and mitigation of the geohazard risks.

This study first reviews the unloading-induced faulting cases associated with underground space development and natural resource extraction. Both rock and fluid mass removals modify local stresses and may cause fault instability. Underground space creation perturbs faults and fractures at shallow depths and requires permanent support for civil uses, whereas resource extraction at great depths influences mainly on the stability of pre-existing faults if hydraulic fracturing is not involved. Some unusual cases are subsequently highlighted, in terms of non-uniform distribution of shear stress along faults, unexpected geohazard from undetected faults, and transition between stick slip and stable sliding. Many theoretical and practical methods related to seismic moment prediction and geological hazard mitigation are discussed at the end.

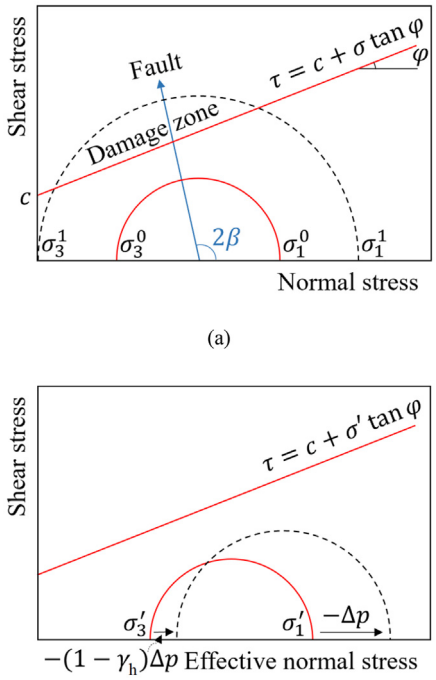

Fig. 1. Changes of principal stresses on the fault before (solid red circle) and after (dashed black circle) unloading activities (after van Wees et al., 2014; Duan et al., 2019). (a) Maximum (σ_1) and minimum (σ_3) principal stresses change to enlarge the Mohr circle, and (b) changes of principal stresses shift the enlarged circle. Here σ' is the effective normal stress, τ is the critical shear stress, Δp is the change in pore pressure, γ_h is the stress path parameter, c and φ are the cohesion and friction angle of the fault, respectively.

2 Fault instability induced by underground space development

Fault instability due to tunnel and cavern excavation in deep rocks has become noticeable due to a rising demand for subsurface infrastructure as well as energy and waste storage. In rock engineering, excavation-induced fault slip is considered as one of the main types of rock burst (Ortlepp & Stacey, 1994). Particularly, this type of rock burst may cause larger seismic events than the other types, probably because the excavation-induced slip of a local segment perturbs other segments beyond the excavation disturbed zone. The local segment should approach failure and favor strain energy accumulation (Manouchehrian &

Cai, 2018). A sudden release of accumulated strain energy mainly controls the intensity of seismic waves (Sainoki & Mitri, 2014) and leads to fault asperity degradation and dislocation or even catastrophic failure of adjacent rocks (Zhou et al., 2015). However, large seismic events may not always be linked to fault slip. Some seismic events are correlated to stress concentration in fractured rocks but not to strong faults (Snelling, Godin, & McKinnon, 2013).

Possible causes of excavation-induced fault instability include reduction and rotation of in situ stresses on a pre-existing fault. The reductions in normal and shear stresses on a sheared fault have been observed in many studies (e.g., Wu, Zou, Li, & Zhao, 2014; Meng et al., 2017). When the fault approaches failure, both the normal and shear stresses sharply drop due to interparticle force reduction and particle contact breakage (Wu et al., 2017). The fault failure is dependent on in situ stress and unloading process. A higher normal stress and a lower shear stress provide a favorable environment for strain energy accumulation, and a larger normal stress unloading rate promotes strain energy release and fault slip displacement. As shown in Fig. 2, the dramatic reduction in normal stress due to tunnel excavation is one of the primary reasons for fault instability during the construction of the Gotthard Base Tunnel. Moreover, the reduction rate of shear stress on the fault is lower than that of normal stress to accelerate the fault failure. The reduction in normal stress is associated with high and/or unfavorably re-oriented stresses, geometry of underground openings, as well as excavation rate and direction relative to principal stresses (Keneti & Sainsbury, 2018).

Stress rotation has been identified as a possible reason for the instability of natural faults (Hardebeck & Michael, 2004) and mainly influences the strength of unfavorably oriented faults (Faulkner, Mitchell, Healy, & Heap, 2006). In rock engineering, fault instability due to stress rotation has been rarely reported (e.g., Snelling et al., 2013). However, in some cases, the concept of stress rotation well interprets the occurrence of fault instability, such as one of the largest fault slip events in the Jinping II hydropower station project in China (Duan, Ji, Xu, Wan, & Wu, 2019). Figure 3 illustrates a possible change in stress orientation along a pre-existing fault from the far field to an excavated tunnel. The minimum principal stress at the tunnel perimeter approaches zero, and the maximum principal stress is vertical. The radius of the Mohr circle is thus enlarged, resulting in the circle partially exceeding the failure envelope (Fig. 1(a)). Therefore, the fault most likely becomes favorably oriented, because the fault orientation readily falls in the damage zone above the failure envelope.

Few studies have reported detailed observations of excavation-induced fault instability in the field (e.g., Xu et al., 2016). Laboratory studies are commonly used as analogs to explore the mechanisms behind fault instability, but a handful of such studies consider stress unloading conditions (Table 1). Also, it is critical to understand similarities and differences between the field and laboratory investigations. McGarr (1994) compares the mining-induced and laboratory seismic events and reveals similar slip behaviors, in which released strain energy is mostly consumed to overcome friction. However, a small-scale fault in the laboratory exhibits a homogenous slip over a decreasing area between two overlapped surfaces, whereas a large-scale fault in the field appears an inhomogeneous slip containing aseismic slip and no slip on some local segments. The seismic efficiency for a laboratory seismic event is approximately constant and independent of seismic moment, while that for a field seismic event is strongly related to seismic moment. Therefore, multi-scale slip heterogeneity should be taken into account when laboratory results are used to explain field observations.

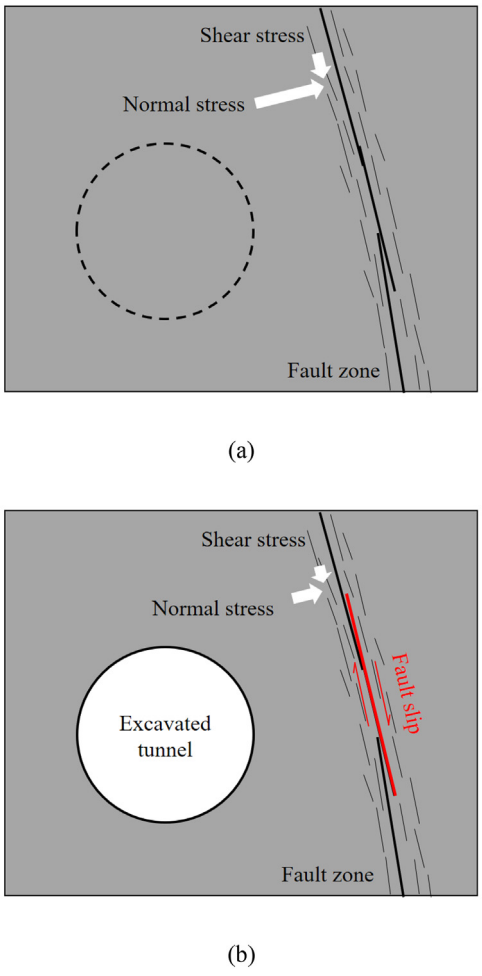

Fig. 2. Possible changes of normal and shear stress magnitudes on the fault (a) before and (b) after tunnel excavation (after Wu et al., 2017).

3 Fault instability induced by natural resource extraction

Fault instability can be induced by stress perturbation due to the extraction of natural resources, such as coal, groundwater, hydrocarbons, and geothermal fluid. These

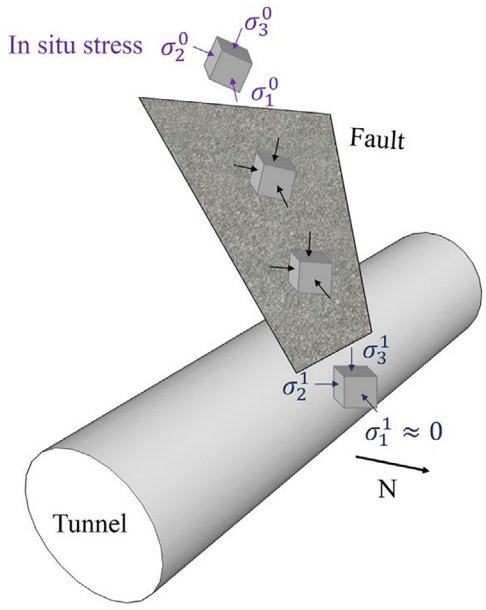

Fig. 3. Possible changes of principal stress orientations of the fault from the far-field to periphery of an excavated tunnel (after Duan et al., 2019).

anthropogenic seismic events have been reviewed by Foulger et al. (2018), and a comprehensive summary can be found in the *HiQuake* database (Wilson, Foulger, Gluyas, Davies, & Julian, 2017). This study sheds light on a few key factors controlling unloading-induced fault instability, such as mining depth, pore pressure, stress distribution, and production rate from a view of rock mechanics (Table 2).

Mining depth significantly influences the occurrence and consequence of unloading-induced fault instability. The 1994 M_W 4.3 earthquake at the Cacoosing Valley in southeastern Pennsylvania, the United States occurred at a shallow depth (<2 km) below a quarry. The removal of overburden caused a reverse fault dictating with joint sets in shallow rocks and approaching failure (Seeber, Armbruster, Kim, Barstow, & Scharnberger, 1998). This earthquake resulted in serious damage to surface infrastructures because of the shallow source depth. The disturbed range of deep mines is found between the floor lower bound depth and floor upper bound depth (Fig. 4). Rock burst most likely occurs between the bound depths, and fault instability can be induced readily within this range (Li, Cai, & Cai, 2007). However, it is very difficult to estimate the bound depths, which depend on rock strength and in situ stress. For example, the Taiji coal mine in Liaoning Province, China initiates from 0.5 km deep and finally reaches 7 km, and the floor lower bound depth is about 6 km.

Extensive groundwater extraction unloads the crustal stress and causes fault instability and ground subsidence. A possible mechanism of the 2017 M_W 7.3 Iran–Iraq border earthquake is shown in Fig. 5. The water depressurization induces an extra horizontal stress on the fault, which is about 10% of the secular interseismic stress change and accelerates reverse faulting (Kundu et al., 2019). Similarly, the 2015 M_W 7.8 Gorkha earthquake in Nepal is attributed to an additional component of horizontal compression at the hypocentral depth (Kundu et al., 2015). Another example is the 2011 M_W 5.1 Lorca earthquake in Spain, which is due to crustal unloading associated with groundwater extraction (González, Tiampo, Palano, Cannavó, & Frenandez, 2012). The fault rupture may nucleate owing to the unloading stress at the upper frictional transition of a seismogenic layer and extend into a velocity-strengthening zone near the surface.

Extraction of natural oil and gas modifies the in situ stresses within and beyond the reservoirs, leading to fault formation and seismic deformation. As shown in Fig. 6, reverse faulting occurs above and below the reservoirs, and normal faulting develops on the reservoir flanks (Segall, 1989). The 1983 M_W 6.5 Coalinga, 1985 M_W 6.1 Kettleman North Dome, and 1987 M_W 5.9 Whittier Narrows earthquakes that occurred below the major oil fields in California, the United States are attributed to stress imbalance on the upper crust caused by oil production, which is linked to the total seismic moment (McGarr, 1991). Figure 7 depicts that the vertical stress imbalance results in fault formation/extension and seismic/aseismic deformation. Additionally, oil and gas extraction reduces pore pressure and amplifies effective normal stress, which should not directly induce fault instability but perturb regional stress fields. Hence, the seismic events can be triggered at large distances from the reservoirs (Grasso, 1992). At the Lacq gas field in France, over 2000 seismic events with $M_L < 4.2$ due to natural gas extraction were recorded from 1974 to 1997 (Bardainne, Dubos-Sallée, Sénéchal, Gaillot, & Perroud, 2008). The gas pressure reduced from 66 MPa in 1957 to 2.3 MPa in 2008, accompanied by surface subsidence up to 6 cm. The surface subsidence and faulting process can be explained by Odonne, Ménard, Massonnat, and Rolando (1999) in which the steep nodal planes extend from the reservoir to the ground surface to promote surface subsidence (Fig. 8). The 1992 $M_W \sim 5.4$ earthquake that occurred at the Groningen gas field in the Netherland is attributed to the interaction between the initial stress and differential compaction (van Wees et al., 2014). The differential compaction due to gas depletion can also explain the delay of earthquake occurrence and the increase in seismic moment. Based on the reservoir and seismic data from the Netherlands, van Eijs et al. (2006) identify three key parameters, including pressure drop, fault density, and stiffness ratio between seal and reservoir rocks, which correlate well with the occurrence of induced earthquakes. One of the largest induced seismic events associated with the extraction of natural gas occurred at the Gazil Reservoir, Uzbekistan (Simpson & Leith, 1985). The 1984 surface wave magnitude (M_S) ~ 7.0 and two former earthquakes with similar magnitudes were induced by fault rupture extending downward, which may interact with blind faults mainly controlled by the tectonic stress. The complex faulting process could explain the

Table 1
Experimental studies on unloading-induced fault instability.

Experimental setup	Rock type and fault property	Initial stress condition	Unloading condition	Failure mechanism	Reference
Analog model	Dry sand	Gravity of sand layers	Deflation of balloon	Development of steep reverse faults	(Odonne et al., 1999)
Direct-shear setup	Norite, quartz sand gouge	Normal stress 2–6 MPa and shear stress 0.25–0.75 MPa	Normal stress unloading rate 0.04–1.98 MPa/s	Both normal and shear stresses drop when the fault approaches a critical stress state	(Wu et al., 2017)
Triaxial shear-flow setup	Granite, smooth and natural fractures	Normal stress 26 MPa and shear stress 0.25–0.75 MPa	Normal stress unloading rate 0.005–0.05 MPa/s	Relationship between the test system stiffness and fault slip weakening rate controls fault instability	(Ji et al., 2019)
Direct-shear setup	Polycarbonate, smooth and rough fractures	Normal stress 2.5 MPa and shear velocity 10 μm/s	Reduction in normal stress 0.2 MPa/step	Transition between stick slip and stable sliding	(Mei & Wu, 2021)

occurrence of three major earthquakes and the geometry of an immature fault network (Bossu et al., 1996).

Most of the seismic events that occur in the geothermal fields are related to fluid injection associated with hydraulic fracturing (Ji & Wu, 2020; Schultz et al., 2020). In contrast to fluid injection, the extraction of hot fluids not only decreases pore pressure in geothermal reservoirs but also induces thermal stress due to temperature drop. Both fluid injection and extraction are possible to cause an increase in seismic rate. The anthropogenic seismic events at the Cerro Prieto geothermal field in Mexico show a strong correlation between the seismic moment and production increase (Glowacka & Nava, 1996). The geothermal field is located between two critically stressed faults in a tectonically active area. The production increase thus readily produces significant stress changes in this area, such as a dramatic decrease in pore pressure, causing a high probability of earthquake occurrence. Meanwhile, the coupled thermo-hydro-mechanical-chemical process can modify the stresses on these faults through pore pressure diffusion, temperature alteration, and stress-aided corrosion to promote the earthquake occurrence (Rathnaweera, Wu, Ji, & Gamage, 2020).

4 Lessons from unusual cases

Many cases in previous sections have shown that stress evolution is accompanied by unloading-induced fault instability and can be explained by the Mohr–Coulomb failure criterion. These cases can be reproduced and analyzed using numerical models, such as finite and discrete element models (Table 3). However, some cases may not be well interpreted according to our current knowledge and models, and further investigations are needed to improve our understanding of the mechanisms behind. This section highlights three such cases, including non-uniform distribution of shear stress along faults, unexpected geohazard from undetected faults, and transition between stick slip and stable sliding.

When unloading activities influence local stresses on a fault segment, the shear stress along the fault can evolve non-uniformly to induce fault rupture in the near field. The fault rupture may propagate subsequently beyond unloading-disturbed rocks and perturb other segments tectonically controlled in the far field, resulting in damaging earthquakes. The mine-induced fault instability at the Sudbury Structure in Canada was triggered remotely by underground excavation, which was located beyond critically stressed faults and caused intermittent slip to activate the faults (McKinnon, 2006). For the Craig Haulage Drift at Strathcona Mine in Canada, fault creep occurred due to an elevated shear stress and induced rock buckling and violent burst (Ortlepp & Stacey, 1994). At the Rudna copper mine in Poland, a positive stress change of over 5 kPa can contribute to the seismic generation process and influence the future seismic rate (Orlecka-Sikora, 2010). The non-uniform distribution of shear stress along the fault

Table 2
Typical fault instability cases induced by natural resource extraction.

Target resource	Magnitude type	Depth (km)	Location	Time	Failure mechanism	Reference
Coal and gold	M_L 2.5	3.3	Boksburg, South Africa	1972	Tremors due to normal faulting	(McGarr, 1976)
	M_L 4.3	0.6	Beipiao, China	1977	Mining-induced fault slip	(Li et al., 2007)
	M_W 4.3	2	Reading, the United States	1994	Shallow fault dictates with joint sets	(Seeber et al., 1998)
	M_L 2.7	1	Yima, China	2010	Mining-induced fault slip burst	(Lu et al., 2019)
Groundwater	M_W 5.1	2–4	Lorca, Spain	2011	Crustal stress unloading due to groundwater extraction	(González et al., 2012)
	M_W 7.8	15	Gorkha, Nepal	2015	Overburden unloading due to groundwater extraction amplifies horizontal compression	(Kundu et al., 2015)
	M_W 7.3	19	Iran–Iraq border	2017	Similar to Gorkha, Nepal	(Kundu et al., 2019)
Oil and gas	M_L 4.2	3.2	Lacq, France	1974–1997	Faults well oriented to achieve stress perturbation during gas extraction	(Bardainne et al., 2008)
	M_W 6.5, 6.1, 5.9	10	Coalinga, Kettleman North Dome, and Whittier Narrows, the United States	1983, 1985, 1987	Earthquake sequences attributed to stress imbalance due to oil production	(McGarr, 1991)
	M_S 7	9	Gazil, Uzbekistan	1984	Blind fault intersects with Gazil gas field	(Simpson & Leith, 1985)
	M_W 5.4	17	Groningen, the Netherlands	1992	Differential compaction of faulted reservoirs	(van Wees et al., 2014)
Geothermal	M_L 6.6	10	Imperial Valley, Mexico	1979	Strong correlation between geothermal production and seismic events	(Glowacka & Nava, 1996)

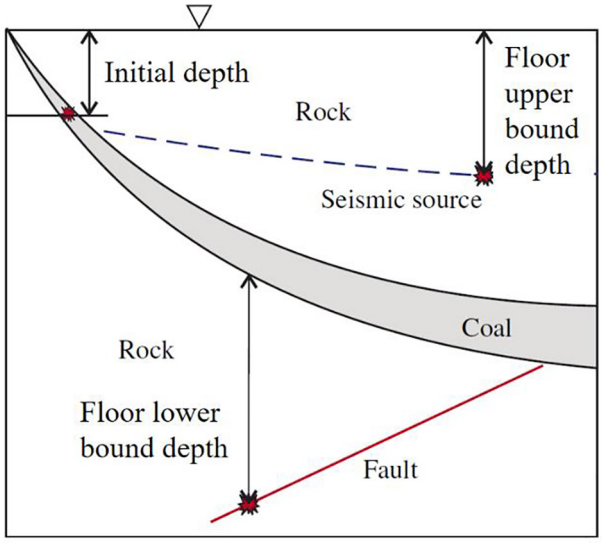

Fig. 4. Floor upper and lower bound depths above and below deep mines (after Li et al., 2007).

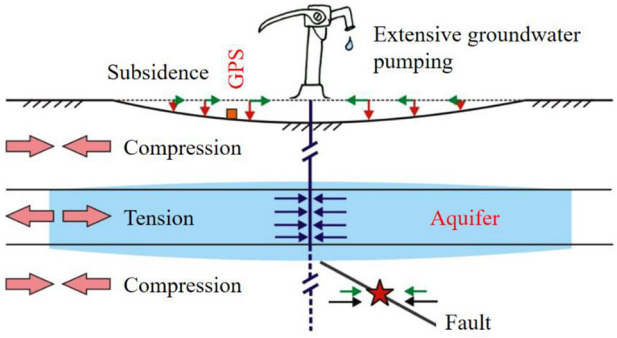

Fig. 5. Crustal unloading, surface subsidence, and fault instability due to groundwater extraction (after Kundu et al., 2019).

can also be promoted by rock mass creep (e.g., relaxation deformation of faults) and influence the long-term stability of underground structures (Song, Cai, Feng, Chen, & Wang, 2011).

Perturbation of undetected faults is often encountered in rock engineering, and the cases with minor faults are mostly negligible. However, the unloading-induced instability of major faults close to project sites may lead to destructive geohazards. In the Jinping II hydropower station project in China, an extremely intense fault slip burst occurred in 2009 during the construction of a drainage tunnel, and a tunnel boring machine was fully destroyed due to rock collapse (Zhang, Feng, Zhou, Qiu, & Wu, 2013). An undetected fault near the tunnel roof was recognized after the rock collapse, and the failure process associated with the presence of the fault was confirmed by Manouchehrian and Cai (2018). The seismic events induced by the instability of undetected faults have not been thoroughly studied because of challenges in model setup and calibration. Adequate geological and geophysical investigations at project sites, particularly accurate identification of nearby major faults, are thus critical to ensure the safety and success of rock engineering projects.

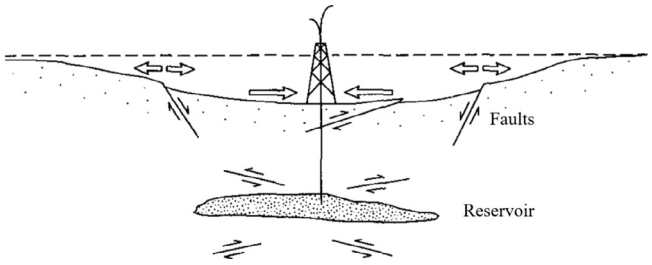

Fig. 6. Surface deformation and formations of normal and reverse faults due to fluid withdrawal (after Segall, 1989).

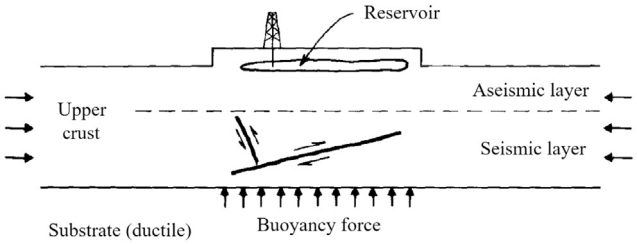

Fig. 7. Fault instability in seismic layer and surface uplift in aseismic layer due to fluid removal (after McGarr, 1991).

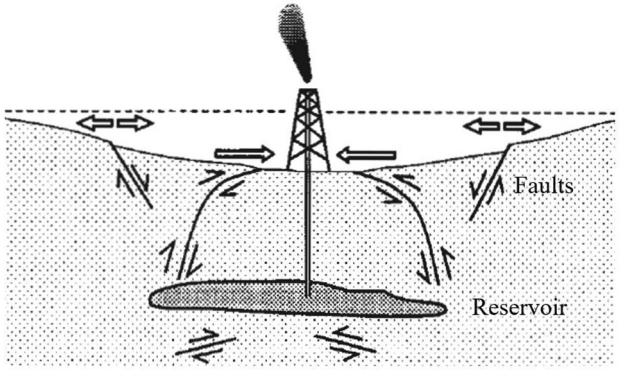

Fig. 8. Steep fault planes extend from the reservoir to the ground and cause surface deformation due to fluid withdrawal (after Odonne et al., 1999).

Stick slip and stable sliding are the most commonly observed behaviors of a pre-existing fault. Stick slip occurs when the elastic stiffness of surrounding rocks is less than a critical rheologic stiffness of the fault, whereas stable sliding appears in stiffer surrounding rocks (Leeman, Saffer, Scuderi, & Marone, 2016). Stick slip has been recognized as a mechanism of earthquakes (Brace and Byerlee, 1996) and detected readily using microseismic monitoring (Cai, Kaiser, & Martin, 2001). However, the fault may slide silently and be accompanied by undetectable strain energy release. Recent observations on the San Andreas Fault in California reveal that a transition between stick slip and stable sliding (Shelly, 2010; Veedu & Barbot, 2016), which may be a clue in predicting the occurrence of stable sliding. A series of direct-shear experiments on a simulated, sawcut fault in polycarbonate was conducted to reproduce a transition from stick slip to stable sliding under decreasing normal stress at a constant slip velocity (Mei & Wu, 2020). The transition is characterized by the alternative occurrence of small and large shear stress drops and attributed to the distinct evolution of asperity contacts under a narrow range of normal stress (Fig. 9). However, detection of this transition could be challenging in nature, as the unusual slip behavior may be difficult to isolate from complex slip behaviors of heterogeneous faults.

5 Prediction and mitigation of fault instability

Many theoretical and practical methods have been proposed to predict and mitigate fault instability during underground space creation and resource extraction. However, most of these methods are derived from specific laboratory and field cases, and assumption and applicability should be further checked for other cases with different geological and engineering settings.

A well-known relationship between the total seismic moment (ΣM_0) and volume change (ΔV) (e.g., rock and fluid mass removals) is proposed by McGarr (1976):

$$\sum M_0 = G\Delta V, \tag{2}$$

where G is the modulus of rigidity.

To estimate the total seismic moment using this relationship, changes in shear stress must exceed some thresholds associated with notable ground deformation before the occurrence of the seismic events (McGarr, Spottiswoode, & Gay, 1975). Also, the permeability of rocks should be very low and not be disturbed by fluid withdrawal. The total seismic moments estimated from the volume of rocks mined in the East Rand Proprietary Gold Mine in South Africa agree well with those measured from mine tremors (McGarr, 1976).

The total seismic moment due to mass removal (Δm) can be estimated as (McGarr, 1991):

$$\sum M_0 = 2G\Delta m\gamma/\rho_c, \tag{3}$$

where γ is the fraction of the upper crust that is seismogenic, and ρ_c is the average crustal density.

The Coalinga, Kettleman North Dome, and Whittier Narrows earthquakes caused by oil production validate the applicability of this equation and the mechanism described in Fig. 8. The interaction between the seismic layer and ductile substrate controls the seismic deformation, but the corresponding response of the substrate to the stress imbalance is not verified in this study.

Given the fact that the critical shear stress (τ_c) of a normally unloaded fault is equal approximately to the residual shear strength of a constantly sheared fault observed from a series of triaxial shear experiments, Ji et al. (2019) derive the normal stress reduction ($\Delta\sigma_n$) required to activate the fault and the maximum seismic moment (M_0) as a function of normal stress reduction:

Table 3
Numerical studies on unloading-induced fault instability.

Numerical method	Rock type	Initial stress condition	Loading/ unloading condition	Failure mechanism	Reference
Finite difference method (FLAC2D)	Hard rock (granite and metasedimentary rocks)	Major principal stress 47.9 MPa and minor stress 2.1 MPa	Boundary gridpoint velocity vector $< 10^{-5}$ m/step	Remote triggering of seismicity from relatively minor disturbance	(McKinnon, 2006)
Finite difference method (FLAC3D)	Ore	Vertical stress 79–87 MPa	Normal stress release rate 0.001–0.1	Intense shock pulses from unloading of fault asperities	(Sainoki & Mitri, 2014)
Discrete element method (PFC2D)	Norite, quartz sand gouge	Normal stress 2–6 MPa and shear stress 0.25–0.75 MPa	Upper wall moving velocity 0.0005–0.005 m/s	Stress reduction due to interparticle force decrease and particle contact breakage	(Wu et al., 2017)
Finite element method (Abaqus2D)	Marble	Vertical stress 60 MPa and horizontal stress 30 MPa	Reduction of contact stiffness between element from 20 GN/m to 0 in 10 steps	Critically positioned and oriented faults promote fault slip burst occurrence	(Manouchehrian & Cai, 2018)
Discrete element method (PFC2D)	Granite	Confining pressure 20 MPa	Axial displacement rate 0.001 mm/s	Change of the angle between maximum principal stress orientation and fault orientation from far field to tunnel periphery	(Duan et al., 2019)
Boundary element method	Hard rock	Vertical stress 20 MPa	Angle of the position for slip initiation	Arrest and runaway ruptures from a near-excavation fault	(Yang et al., 2020)
Finite difference method (FLAC3D)	Granite/gneiss	Vertical stress 13.24 MPa and horizontal stress 7.95 MPa	Reduction in effective normal stress	Runway rupture extending to the entire fault	(Rinaldi & Urpi, 2020)

$$\Delta\sigma_n = \frac{\Delta\tau}{\mu} = \frac{\tau_s - \tau_c}{\mu}, \tag{4}$$

$$M_0 = \frac{16\mu R^3}{7}\Delta\sigma_n, \tag{5}$$

where $\Delta\tau$ is the shear stress drop, τ_s is the shear strength, and R is the radius of the fault.

Equation (5) can well predict the maximum seismic moments of the dry and saturated faults with known fault sizes in the laboratory. However, in the field, the reliability of this equation depends highly on accurate estimation of fault size, which can be evaluated from microseismic monitoring (Kuang, Zoback, & Zhang, 2017).

Many field studies have identified the characteristics of fault instability based on microseismic measurement. For instance, if the ratio of the S-wave energy to P-wave energy is larger than 10, fault slip likely occurs (Gibowicz, Young, Talebi, & Rawlence, 1991; Dai, Li, Xu, Fan, & Zhang, 2016). Prior to fault instability, decreases in b value and energy release are observed in a few cases (Zhang et al., 2015; Liu et al., 2020), which are attributed to relatively large seismic events occurring along the fault and less damage in adjacent rocks. Also, the dominant frequency of microseismic signals becomes lower, and the apparent stress is higher (Lu, Dou, Liu, Xie, & Liu, 2012; Zhang et al., 2015). Some of these changes are recognized as precursors in post-data analyses. However, under extremely complex engineering conditions, it is still challenging to correlate such changes with coming geohazards and to rule out other factors that also link to these changes. Some changes may appear before, during, and after the geohazards in different cases. Hence, our ability to predict fault instability remains inadequate, and our understanding should be improved further to establish reliable early warning systems. To mitigate the seismic events, some options could be usable, including releasing strain energy using preconditioning techniques (Toper, Kabongo, Stewart, & Daehnke, 2000), constraining fault slip using reinforcement structures (Zhang, Feng, Zhou, Qiu, & Wu, 2012), and maintaining fluid pressure in hydrocarbon reservoirs (Rutledge, Phillips, & Schuessler, 1998). A list of mitigation measures (e.g., sealing of the face with steel-fiber shotcrete, face anchors with large anchor plates) is used during the construction of the Gotthard Base Tunnel (Rehbock-Sander & Jesel, 2018). Alternatively, uncertainties (e.g., degree of belief) and indicators (e.g., surface distortion) can be used to analyze the probability of the geohazard risks (Einstein, 1996).

Recent advances in data analytics and machine learning offer us robust tools to mitigate the geohazard risks.A traffic light system has been used successfully to monitor and control the induced seismic events during hydraulic fracturing and wastewater disposal (Bommer et al., 2006; Walters, Zoback, Baker, & Beroza, 2015). The real-time, forward-looking and probabilistic system

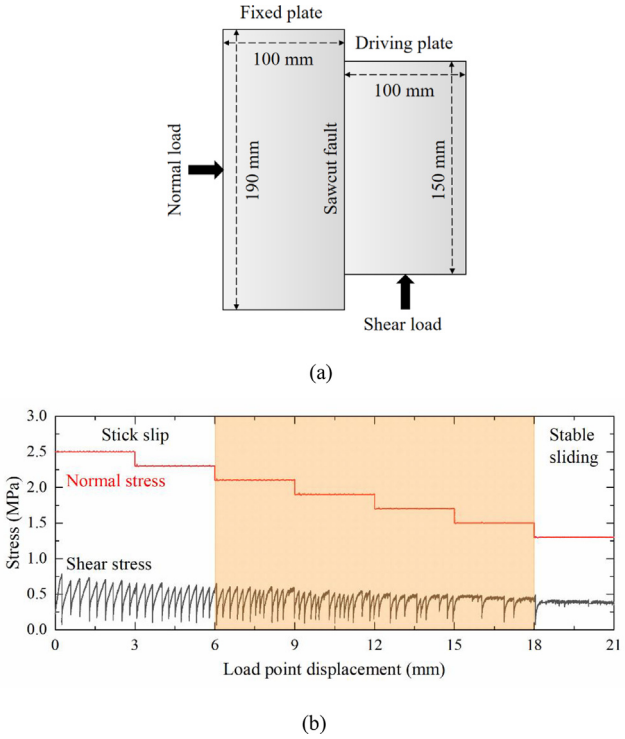

Fig. 9. (a) Direct-shear experiments on a simulated fault with a thickness of 9.3 mm, and (b) transition stage between stick slip and stable sliding highlighted in orange background (after Mei & Wu, 2020).

includes three hazard levels based on the seismic event size, ground velocity magnitude, and public response, and provides reliable references for earthquake forecast and decision making (Király-Proag et al., 2016). This system can be used readily to predict the occurrence of the induced seismic events in other underground projects (e.g., tunnel and cavern excavation), in which the seismic sensors have been installed for rock burst monitoring. The poorly sampled, massive amount of seismic data can be processed efficiently and used effectively through machine learning to improve the early warning of induced earthquakes and to extract useful data from unseen signals. Machine learning has been used successfully for earthquake detection and location in Oklahoma, the United States (Perol, Gharbi, & Denolle, 2018), especially for small earthquakes based on a low signal-to-noise ratio in data (Zhang et al., 2020). As shown in Fig. 10, the future application of machine learning should combine with physical modelling to develop a hybrid approach for data-driven insights (Kong et al., 2019).

6 Concluding remarks

Unloading-induced fault instability is a traditional topic in rock engineering but attracts more attention when deep underground space and resource become our emerging needs in recent years. At great depths, large-scale faults could play more important roles in rock instability, as small-scale fractures are less encountered and their movements can be restricted under high stress conditions. Fault activation induced by rock and fluid removals can be mostly explained by the Mohr–Coulomb failure criterion, but some cases are exceptional, such as polymodal faulting. Excavation-induced fault instability can be caused by reduction and rotation of in situ stresses on pre-existing

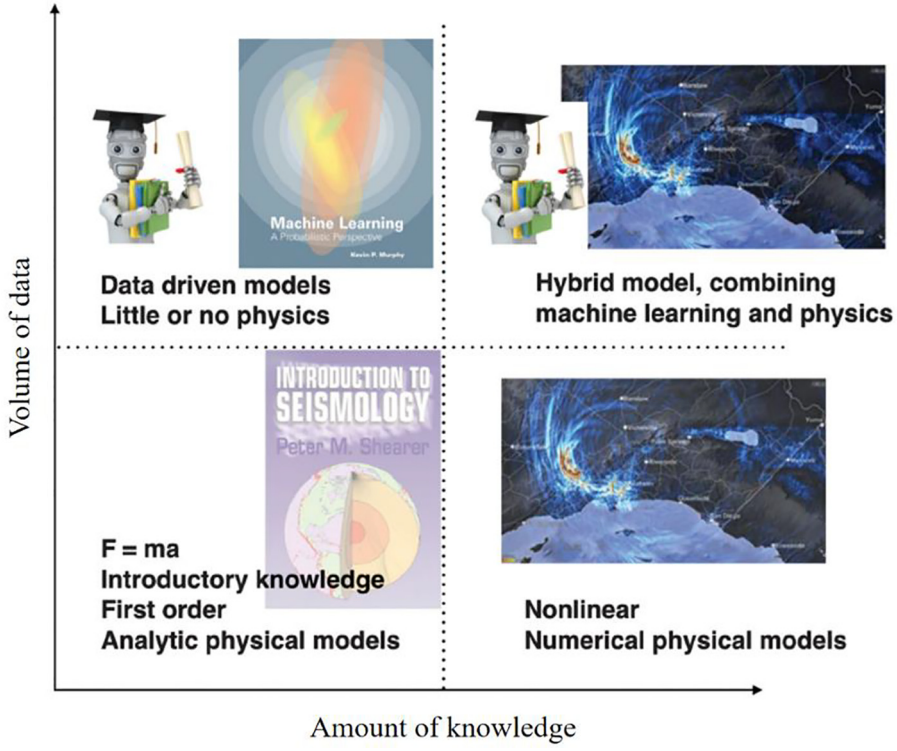

Fig. 10. Development of hybrid model by combining physical, machine learning-based and data-driven models (after Kong et al., 2019).

faults, and fault instability due to resource extraction can be related to mining depth, pore pressure, stress distribution, and production rate. Some challenges remain, like how to control remote triggering of fault instability and how to manage unseen threat of undetected fault. Emerging technologies, such as data analytics and machine learning combining with physical and data-driven models, could provide new avenues for predicting and mitigating the anthropogenic geohazards. Moreover, multi-scale slip heterogeneity should be considered when laboratory simulations are used to interpret field observations.

Declaration of Competing Interest

The author declare that he has no known competing financial interests or personal relationships that could have appeared to influence the work reported in this paper.

Acknowledgement

The author gratefully acknowledges the support of Start-up Grant from Nanyang Technological University, Singapore.

References

Bardainne, T., Dubos-Sallée, N., Sénéchal, G., Gaillot, P., & Perroud, H. (2008). Analysis of the induced seismicity of the Lacq gas field (Southwestern France) and model of deformation. *Geophysical Journal International, 172*, 1151–1162.

Brace, W. F., & Byerlee, J. D. (1996). Stick-slip as a mechanism for earthquakes. *Science, 153*(3739), 990–992.

Bommer, J. J., Oates, S., Cepeda, J. M., Lindholm, C., Bird, J., Torres, R., ... Rivas, J. (2006). Control of hazard due to seismicity induced by a hot fractured rock geothermal project. *Engineering Geology, 83*(4), 287–306.

Bossu, R., Grasso, J. R., Plotnikova, L. M., Nurtaev, B., Fréchet, J., & Moisy, M. (1996). Complexity of intracontinental seismic faultings: The Gazli, Uzbekistan, sequence. *Bulletin of the Seismological Society of America, 86*(4), 959–971.

Cai, M. (2008). Influence of intermediate principal stress on rock fracturing and strength near excavation boundaries – insight from numerical modeling. *International Journal of Rock Mechanics and Mining Sciences, 45*(5), 763–772.

Cai, M., Kaiser, P. K., & Martin, C. D. (2001). Quantification of rock mass damage in underground excavation from microseismic event monitoring. *International Journal of Rock Mechanics and Mining Sciences, 38*(8), 1135–1145.

Candela, T., Osinga, S., Ampuero, J. P., Wassing, B., Pluymaekers, M., Fokker, P. A., ... Muntendam-Bos, A. G. (2019). Depletion-induced seismicity at the Groningen Gas Field: Coulomb rate-and-state models including differential compaction effect. *Journal of Geophysical Research: Solid Earth, 124*(7), 7081–7104.

Cook, N. G. W. (1976). Seismicity associated with mining. *Engineering Geology, 10*(2–4), 99–122.

Dai, F., Li, B., Xu, N., Fan, Y., & Zhang, C. (2016). Deformation forecasting and stability analysis of large-scale underground powerhouse caverns from microseismic monitoring. *International Journal of Rock Mechanics and Mining Sciences, 86*, 269–281.

Dou, Z., Gao, T., Zhao, Z., Li, J., Yang, Q., & Shang, D. (2020). The role of water lubrication in critical state fault slip. *Engineering Geology, 271*, 105606.

Duan, K., Ji, Y., Xu, N., Wan, Z., & Wu, W. (2019). Excavation-induced fault instability: Possible causes and implications for seismicity. *Tunneling and Underground Space Technology, 92*, 103041.

Einstein, H. H. (1996). Risk and risk analysis in rock engineering. *Tunneling and Underground Space Technology, 11*(2), 141–155.

Ellsworth, W. L. (2013). Injection-induced earthquakes. *Science, 341* (6142), 1225942.

Faulkner, D. R., Mitchell, T. M., Healy, D., & Heap, M. J. (2006). Slip on 'weak' faults by the rotation of reginal stress in the fracture damage zone. *Nature, 444*, 922–925.

Foulger, G. R., Wilson, M. P., Gluyas, J. G., Julian, B. R., & Davies, R. J. (2018). Global review of human-induced earthquakes. *Earth-Science Reviews, 178*, 438–514.

Gane, P. G., & Oliver, H. A. (1946). A seismic investigation of the Witwatersr and earth tremors. *Bulletin of the Seismological Society of America, 36*(2), 49–80.

Glowacka, E., & Nava, F. A. (1996). Major earthquakes in Mexicali Valley, Mexico, and fluid extraction at Cerro Prieto geothermal field. *Bulletin of the Seismological Society of America, 86*(1A), 93–105.

Gibowicz, S. J., Young, R. P., Talebi, S., & Rawlence, D. J. (1991). Source parameters of seismic events at the Underground Research Laboratory in Maniboba, Canada: Scaling relations for events with moment magnitude smaller than −2. *Bulletin of the Seismological Society of America, 81*(4), 1157–1182.

González, P. J., Tiampo, K. F., Palano, M., Cannavó, & Frenandez, J. (2012). The 2011 Lorca earthquake slip distribution controlled by groundwater crustal unloading. *Nature Geoscience*, 5(11), 821–825.

Grasso, J. R. (1992). Mechanics of seismic instabilities induced by the recovery of hydrocarbons. *Pure and Applied Geophysics, 139*(3/4), 507–534.

Hardebeck, J. L., & Michael, A. J. (2004). Stress orientations at intermediate angles to the San Andreas Fault. *California. Journal of Geophysical Research, 109*, B11303.

Healy, D., Blenkinsop, T. G., Timms, N. E., Meredith, P. G., Mitchell, T. M., & Cooke, M. L. (2015). Polymodal faulting: Time for a new angle on shear failure. *Journal of Structural Geology, 80*, 57–71.

Husen, S., Kissling, E., & von Deschwanden, A. (2013). Induced seismicity during the construction of the Gotthard Base Tunnel, Switzerland: Hypocenter locations and source dimensions. *Journal of Seismology, 17*(1), 63–81.

Ji, Y., Wu, W., & Zhao, Z. (2019). Unloading-induced rock fracture activation and maximum seismic moment prediction. *Engineering Geology, 262*, 105352.

Ji, Y., & Wu, W. (2020). Injection-driven fracture instability in granite: Mechanism and implications. *Tectonophysics, 791*, 228572.

Keneti, A., & Sainsbury, B. A. (2018). Review of published rockburst events and their contributing factors. *Engineering Geology, 246*, 361–373.

Király-Proag, E., Zechar, J. D., Gischig, V., Wiemer, S., Karnounis, D., & Doetsch, J. (2016). Validating induced seismicity forecast models – induced seismicity test bench. *Journal of Geophysical Research: Solid Earth, 121*(8), 6009–6029.

Kong, Q., Trugman, D. T., Ross, Z. E., Bianco, M. J., Meade, B. J., & Gerstoft, P. (2019). Machine learning in seismology: Turning data into insights. *Seismological Research Letters, 90*(1), 3–14.

Kuang, W., Zoback, M., & Zhang, J. (2017). Estimating geomechanical parameters from microseismic plane focal mechanisms recorded during multistage hydraulic fracturing. *Geophysics, 82*(1), KS1–KS11.

Kundu, B., Vissa, N. K., & Gahalaut, V. K. (2015). Influence of anthropogenic groundwater in Indo-Gangetic plains on the 25 April 2015 M_W 7.8 Gorkha, Nepal earthquake. *Geophysical Research Letters, 42*(24), 10607–10613.

Kundu, B., Vissa, N. K., Gahalaut, K., Gahalaut, V. K., Panda, D., & Malik, K. (2019). Influence of anthropogenic groundwater pumping on the 2017 November 12 *M*7.3 Iran-Iraq border earthquake. *Geophysical Journal International, 218*(2), 833–839.

Leeman, J. R., Saffer, D. M., Scuderi, M. M., & Marone, C. (2016). Laboratory observations of slow earthquakes and the spectrum of tectonic fault slip modes. *Nature Communications, 7*, 11104.

Li, T., Cai, M. F., & Cai, M. (2007). A review of mining-induced seismicity in China. *International Journal of Rock Mechanics and Mining Sciences, 44*(8), 1149–1171.

Liu, Q., Wu, J., Zhang, X., Tang, L., Bi, C., Li, W., & Xu, J. (2020). Microseismic monitoring to characterize structure-type rockbursts: A case study of a TBM-excavated tunnel. *Rock Mechanics and Rock Engineering, 53*(7), 2995–3013.

Lu, C., Dou, L., Liu, B., Xie, Y., & Liu, H. (2012). Microseismic low-frequency precursor effect of bursting failure of coal and rock. *Journal of Applied Geophysics, 79*, 55–63.

Lu, C., Liu, B., Liu, B., Liu, Y., Wang, H., & Zhang, H. (2019). Anatomy of mining-induced fault slip and a triggered rockburst. *Bulletin of Engineering Geology and the Environment, 78*, 5147–5160.

Manouchehrian, A., & Cai, M. (2018). Numerical modeling of rockburst near fault zones in deep tunnels. *Tunneling and Underground Space Technology, 80*, 164–180.

Mei, C., & Wu, W. (2021). Fracture asperity evolution during the transition from stick slip to stable sliding. *Philosophical Transitions of the Royal Society A*, https://doi.org/10.1098/rsta.2020.0133.

Meng, F., Zhou, H., Wang, Z., Zhang, L., Kong, L., Li, S., ... Hu, S. (2017). Experimental study of factors affecting fault slip rockbursts in deeply buried hard rock tunnels. *Bulletin of Engineering Geology and the Environment, 76*(3), 1167–1182.

McKinnon, S. D. (2006). Triggering of seismicity remote from active mining excavations. *Rock Mechanics and Rock Engineering, 39*(3), 255–279.

McGarr, A. (1976). Seismic moments and volume changes. *Journal of Geophysical Research, 81*(8), 1487–1494.

McGarr, A. (1991). On a possible connection between three major earthquakes in California and oil projection. *Bulletin of the Seismological Society of America, 81*(3), 948–970.

McGarr, A. (1994). Some comparisons between mining-induced and laboratory earthquakes. *Pure and Applied Geophysics, 142*(3/4), 467–489.

McGarr, A., Simpson, D., & Seeber, L. (2002). Case histories of induced and triggered seismicity. *International Handbook of Earthquake and Engineering Seismology, 81A*, 647–661.

McGarr, A., Spottiswoode, S. M., & Gay, N. C. (1975). Relationship of mine tremors to induced stresses and to rock properties in the focal region. *Bulletin of the Seismological Society of America, 65*(4), 981–994.

Odonne, F., Ménard, I., Massonnat, G. J., & Rolando, J. P. (1999). Abnormal reserve faulting above a depleting reservoir. *Geology, 27*(2), 111–114.

Orlecka-Sikora, B. (2010). The role of static stress transfer in mining induced seismic events occurrence, a case study of the Rudna mine in the Legnica-Glogow Copper District in Poland. *Geophysical Journal International, 182*(2), 1087–1095.

Ortlepp, W. D., & Stacey, T. R. (1994). Rockburst mechanisms in tunnels and shafts. *Tunnelling and Underground Space Technology, 9*(1), 59–65.

Perol, T., Gharbi, M., & Denolle, M. (2018). Convolutional neural network for earthquake prediction and location. *Science Advances, 4*(2) e1700578.

Rathnaweera, T. D., Wu, W., Ji, Y., & Gamage, R. P. (2020). Understanding injection-induced seismicity in enhanced geothermal systems: From the coupled thermo-hydro-mechanical-chemical process to anthropogenic earthquake prediction. *Earth-Science Reviews, 205* 103182.

Rehbock-Sander, M., & Jesel, T. (2018). Fault induced rock bursts and micro-tremors – experiences from the Gotthard Base Tunnel. *Tunnelling and Underground Space Technology, 81*, 358–366.

Rinaldi, A. P., & Urpi, L. (2020). Fault reactivation induced by tunneling activity in clay material: Hints from numerical modeling. *Tunnelling and Underground Space Technology, 102*, 103453.

Rutledge, J. T., Phillips, W. S., & Schuessler, B. K. (1998). Reservoir characterization using oil-production-induced microseismicity, Clinton County, Kentucky. *Tectonophysics, 289*(1/2/3), 129–152.

Sainoki, A., & Mitri, H. S. (2014). Simulating intense shock pulses due to asperities during fault-slip. *Journal of Applied Geophysics, 103*, 71–81.

Schultz, R., Skoumal, R. J., Brudzinski, M. R., Eaton, D., Baptie, B., & Ellsworth, W. (2020). Hydraulic fracturing-induced seismicity. *Reviews of Geophysics, 58*(3), e2019RG000695.

Sebik, V. (1963). On securing the safety of operating ore mines exposed to rockburst hazards. In: Proceedings of 3rd International Mining Congress, Salzburg, Austria.

Seeber, L., Armbruster, J. G., Kim, W. Y., Barstow, N., & Scharnberger, C. (1998). The 1994 Cacoosing Valley earthquakes near Reading, Pennsylvania: A shallow rupture triggered by quarry unloading. *Journal of Geophysical Research, 103*(B10), 24505–24521.

Segall, P. (1989). Earthquakes triggered by fluid extraction. *Geology, 17*(10), 942–946.

Shelly, D. R. (2010). Periodic, chaotic, and doubled earthquake recurrence intervals on the deep San Andreas Fault. *Science, 328*(5984), 1385–1388.

Simpson, D. W., & Leith, W. (1985). The 1976 and 1984 Gazil, USSR, earthquakes – were they induced? *Bulletin of the Seismological Society of America, 75*(5), 1465–1468.

Snelling, P. E., Godin, L., & McKinnon, S. D. (2013). The role of geologic structure and stress in triggering remote seismicity in Creighton Mine, Sudbury, Canada. *International Journal of Rock Mechanics and Mining Sciences, 58*, 166–179.

Soltanzadeh, H., & Hawkes, C. D. (2008). Semi-analytical models for stress change and fault reactivation induced by reservoir production and injection. *Journal of Petroleum Science and Engineering, 60*(2), 71–85.

Song, S., Cai, D., Feng, X., Chen, X., & Wang, D. (2011). Safety monitoring and stability analysis of left abutment slope of Jingping I hydropower station. *Journal of Rock Mechanics and Geotechnical Engineering, 3*(2), 117–130.

Toper, A. Z., Kabongo, K. K., Stewart, R. D., & Daehnke, A. (2000). The mechanism, optimization and effects of preconditioning. *The Journal of the South African Institute of Mining and Metallurgy, 100*(1), 7–16.

van Eijs, R. M. H. E., Mulders, F. M. M., Nepveu, M., Kenter, C. J., & Scheffers, B. C. (2006). Correlation between hydrocarbon reservior properties and induced seismicity in the Netherlands. *Engineering Geology, 84*(3/4), 99–111.

van Wees, J. D., Bujize, L., van Thienen-Visser, K., Nepveu, M., Wassing, B. B. T., Orlic, B., & Fokker, P. A. (2014). Geomechanics response and induced seismicity during gas field depletion in the Netherlands. *Geothermics, 52*, 206–219.

Veedu, D. M., & Barbot, S. (2016). The Parkfield tremors reveal slow and fast ruptures on the same asperity. *Nature, 532*(7599), 361–365.

Walters, R. J., Zoback, M. D., Baker, J. W., & Beroza, G. C. (2015). Characterizing and responding to seismic risk associated with earthquakes potentially triggered by fluid disposal and hydraulic fracturing. *Seismological Research Letters, 86*(4), 1110–1118.

Wilson, M. P., Foulger, G. R., Gluyas, J. G., Davies, R. J., & Julian, B. R. (2017). *Hiquake*: The human-induced earthquake database. *Seismological Research Letters, 88*(6), 1560–1565.

Wu, W., Zou, Y., Li, X., & Zhao, J. (2014). An unload-induced direct-shear model for granular gouge friction in rock discontinuities. *Review of Scientific Instruments, 85*(9), 093902.

Wu, W., Zhao, Z., & Duan, K. (2017). Unloading-induced instability of a simulated granular fault and implications for excavation-induced seismicity. *Tunnelling and Underground Space Technology, 63*, 154–161.

Xu, N., Li, T., Dai, F., Zhang, R., Tang, C., & Tang, L. (2016). Microseismic monitoring of strainburst activities in deep tunnels at the Jinping II hydropower station. *China. Rock Mechanics and Rock Engineering, 49*(3), 981–1000.

Yang, J., Yang, D., Zhang, X., Jeffrey, R. G., Chen, W., Sheng, Q., & Zhang, F. (2020). Energy budget and fast rupture on a near-excavation fault: Implications for mitigating induced seismicity. *Journal of Geophysical Research: Solid. Earth, 125*(10), e2020JB019360.

Zhang, C., Feng, X., Zhou, H., Qiu, S., & Wu, W. (2012). A top pilot tunnel preconditioning method for the prevention of extremely intense rockburst in deep tunnels excavated by TBMs. *Rock Mechanics and Rock Engineering, 45*(3), 289–309.

Zhang, C., Feng, X., Zhou, H., Qiu, S., & Wu, W. (2013). Rockmass damage development following two extreme intense rockbursts in deep tunnels at Jinping II hydropower station, southwestern China. *Bulletin of Engineering Geology and the Environment, 72*(2), 237–247.

Zhang, P., Yang, T., Yu, Q., Xu, T., Zhu, W., Liu, H., ... Zhao, Y. (2015). Microseismicity induced by fault activation during the fracture process of a crown pillar. *Rock Mechanics and Rock Engineering, 48*(4), 1673–1682.

Zhang, X., Zhang, J., Yang, C., Liu, S., Chen, Z., & Li, W. (2020). Locating induced earthquakes with a network of seismic stations in Oklahoma via a deep learning method. *Scientific Report, 10*, 1941.

Zhou, H., Meng, F., Zhang, C., Hu, D., Yang, F., & Lu, J. (2015). Analysis of rockburst mechanisms induced by structural planes in deep tunnels. *Bulletin of Engineering Geology and the Environment, 74*(4), 1435–1451.